Supporting Information

Subramanian et al. 10.1073/pnas.1718810115

SI Materials and Methods

Chemostat Growth Conditions. *S. oneidensis* MR-1 cells were grown in continuous flow bioreactors (BioFlo 110; New Brunswick Scientific) with an operating liquid volume of 1 L, as previously described (1–3). A total of 5 mL of a stationary-phase overnight LB culture was injected into the bioreactor containing 1 L of a defined medium (3), while dissolved oxygen tension (DOT) was maintained at 20% by adjusting the ratio of N_2/air mixture entering the reactor (using automatic mode). After 20 h, and as the culture reached stationary phase, continuous flow of the defined medium (3) was started with a dilution rate of 0.05 h^{-1} while DOT was still maintained at 20%. After 48 h of aerobic growth under continuous flow conditions, the DOT was manually reduced to 0% by adjusting the N_2/air mixture entering the reactor. O_2 served as the sole terminal electron acceptor throughout the experiment. pH was maintained at 7.0, temperature at 30 °C, and agitation at 200 rpm to minimize mechanical shear forces [in previous studies (1, 2), chemostat cultures used for *Shewanella* nanowire conductivity measurements were operated at 50 rpm agitation]. Forty hours after DOT reached 0%, samples were taken from the chemostat for TEM imaging.

Batch Culture Growth Conditions. *S. oneidensis* MR-1 was grown overnight in LB broth at 30 °C up to an OD_{600} of 2.4–2.8. A total of 200 μL of this overnight culture was added to each of two duplicates, sealed, and autoclaved in 100-mL serum bottles containing 60 mL of a defined medium (3). One of the two bottles acted as a control and was not used for imaging. To the control bottle, 5 μM resazurin was added to indicate the O_2 levels in the medium. The bottles were then placed in an incubator at 30 °C, with shaking at 150 rpm until the color due to resazurin in the control bottle completely faded, indicating anaerobic conditions. We then took 200 μL of sample from the bottle that did not contain resazurin for TEM imaging.

Negative Stain TEM.

Chemostat. Samples taken from the chemostat were immediately fixed with 2.5% glutaraldehyde and stored at 4 °C. A total of 2 μL of this fixed sample was spotted on a glow-discharged, X-thick carbon-coated, R2/2, Au NH2 London finder Quantifoil EM grid (Quantifoil Micro Tools) and allowed to sit for 2 min. Any remaining liquid was blotted off gently using a kimwipe and the grid was stained with 1% uranyl acetate for 2 min before gently blotting the remaining stain. The grid was then allowed to dry for 1 d at room temperature before imaging in TEM.

Perfusion flow imaging platform. The fixed grid from the perfusion flow imaging platform was blotted to remove excess liquid and stained with 1% uranyl acetate for 2 min before gently blotting the remaining stain. To obtain an fLM image for correlation with EM, the grid was rehydrated with deionized water and reimaged on the inverted fluorescent microscope. The grid was then blotted again and allowed to dry at room temperature before imaging in TEM. Imaging of samples was performed on an FEI 120-keV electron microscope.

ECT Data Analysis and Structure Overlay of MtrC and MtrA on EM Map. The IMOD software package was used for labeling of model points and generating the 3D views presented in Figs. 6 and 7. For Fig. 6 *C–F* (Movie S11 and similar analyses on vesicles from 13 other tomograms), a meshed view of the membrane surface was generated by labeling the membrane as a separate contour in every fifth tomographic slice. This allowed the surface area of the meshed membrane surface to be determined in IMOD. Red and green model points were generated by picking all observed exterior and interior densities, respectively, in every slice of the tomogram. Particles were labeled as cytochromes if they were within ∼5 nm inside or outside of the membrane. Neighboring particles were labeled as separate points only if they were separated by more than ∼5 nm. Particle density was calculated by dividing the number of labeled particles by the membrane surface area. For Fig. 7*C* and Movie S12, the membrane was modeled using a smoothed isosurface model object in IMOD, and all observed densities on the membrane interior and exterior were manually labeled as model points. Density coordinates were extracted and used for distance calculations. The number of model points in Fig. 7*C* is greater than the densities observed in Fig. 7*A* since Fig. 7*C* is a 3D representation of the densities seen in the entire tomogram whereas Fig. 7*A* is a slice from the tomogram that does not contain all of the densities (Movie S12). For Fig. 7*B*, the crystal structure of MtrC was visualized and oriented using UCSF Chimera (4). Adobe Photoshop was then used to overlay this crystal structure onto densities on the EM map. The surface view of MtrA was visualized using the PyMOL software (The PyMOL Molecular Graphics System, Version 1.7.2.0; Schrodinger LLC) and overlaid on EM densities using Adobe Photoshop.

Direct Tunneling Limit Calculation. To find whether direct tunneling is possible between the observed densities in Fig. 7*A*, we used the available structures of MtrC (5) and MtrA (6) to calculate the largest center-to-center intermolecular distance that would allow direct tunneling. From the crystal structure, the dimensions of MtrC are ∼9 × 6 × 4 nm. Since the orientation of MtrC on the OM is unknown, we took the largest dimension (9 nm) to calculate the direct tunneling limit. The known direct tunneling limit for the distance between the donor and acceptor redox sites in biological ET is ∼2 nm (7). This sets the limit of direct tunneling between MtrCs at 11 nm (9 nm + 2 nm) center-to-center intermolecular distance, assuming redox sites are located at the edges of the molecule. In the case of MtrA, the known molecular dimensions are ∼10 × 5 × 2.5 nm. From the EM map, it appears that MtrA is oriented with its long axis (10 nm) perpendicular to the outer membrane (Fig. 7*B*). Therefore, it is likely that any intermolecular electron tunneling between MtrAs occurs along the shorter axes (5 nm and 2.5 nm). Taking the larger of these two dimensions (5 nm), we calculate the limit of direct tunneling between MtrAs to be at 7 nm (5 nm + 2 nm) center-to-center intermolecular distance.

Cytochrome Diffusion and Electron Hopping Rate Calculations. Following the Blauch–Saveant (8) approach for modeling ET in an assembly of redox carriers in two dimensions, the diffusion coefficients for electron hopping between redox carriers (D_e) and the physical motion of redox carriers (D_{phys}) are (8)

$$D_e = \frac{\delta^2}{4t_e}, D_{phys} = \frac{\delta^2}{4t_p}, \quad \text{[S1]}$$

where δ is the center-to-center distance of closest approach between two redox carriers (approximate diameter of one redox carrier), and t_e and t_p are time constants of electron hopping and physical motion, respectively. D_{phys} has been measured for integral membrane proteins similar in size to MtrC to be ∼3 $\mu m^2/s$ (9). Assuming δ to be the average size of MtrC [6.33 nm (5)], we

calculate t_p to be $\sim 3 \times 10^{-6}$ s. D_e can be calculated using t_e, which is estimated by the electron residence time in OM decaheme cytochromes ($\sim 10^{-4}$ s) (10, 11). In the limit where $t_p < t_e$, we use the mean-field expression (Eq. **1**) for the apparent diffusion coefficient (D_{ap}) (8). To calculate the electron flux (J) in an OM extension, we assume a linear drop in the concentration of reduced redox carriers along the OM extension length (L) and that cytochromes are completely reduced at one end and completely oxidized at the other end of the extension:

$$J = D_{ap}\frac{\partial C}{\partial x} \approx D_{ap}\frac{C(x=0) - C(x=L)}{L} = D_{ap}\frac{C_0}{L}. \qquad \textbf{[S2]}$$

Here, C_0 and C represent the total and reduced redox carrier concentrations, respectively. Using Eq. **1** for D_{ap} and assuming a cylindrical OM extension with length L and diameter d, we can find the overall ET rate (I),

$$I = J\pi d = D_{ap}\frac{C_0}{L}\pi d = \frac{C_0}{L}\pi d\left[D_{phys}(1-X)f_c + D_e X\right], \qquad \textbf{[S3]}$$

where the fractional loading (X) is defined as the ratio of cytochrome density to the maximum possible density, C_0/C_{Max}. Assuming spherical redox carriers, C_{Max} can be estimated by the concentration of circles in a hexagonal lattice, C_{Hex}:

$$C_{Max} \approx C_{Hex} = \frac{0.91}{\pi\left(\frac{\delta}{2}\right)^2}. \qquad \textbf{[S4]}$$

Therefore, we can replace C_0 in Eq. **S3** by XC_{Hex}. In addition, the correlation factor f_c in Eq. **1** and Eq. **S3** can be written as (8)

$$f_c = \frac{(2-X)f_{c,X=1}}{2f_{c,X=1} + \left(1 - 2f_{c,X=1}\right)X}, \qquad \textbf{[S5]}$$

where the correlation factor at full fractional loading, $f_{c,X=1}$ is 0.466942 for diffusion in 2D space (8).

Finally, the overall ET rate as a function of redox carrier fractional loading can be written as

$$I(X) = \frac{C_{Hex}}{L}\pi d X\left[D_{phys}(1-X)f_c + D_e X\right]. \qquad \textbf{[S6]}$$

Fig. 8 shows $I(X)$ for MtrC-mediated ET in a cylindrical OM extension with $L = 1$ μm and $d = 100$ nm.

1. Gorby YA, et al. (2006) Electrically conductive bacterial nanowires produced by *Shewanella oneidensis* strain MR-1 and other microorganisms. *Proc Natl Acad Sci USA* 103:11358–11363.
2. El-Naggar MY, et al. (2010) Electrical transport along bacterial nanowires from *Shewanella oneidensis* MR-1. *Proc Natl Acad Sci USA* 107:18127–18131.
3. Pirbadian S, et al. (2014) *Shewanella oneidensis* MR-1 nanowires are outer membrane and periplasmic extensions of the extracellular electron transport components. *Proc Natl Acad Sci USA* 111:12883–12888.
4. Pettersen EF, et al. (2004) UCSF Chimera–A visualization system for exploratory research and analysis. *J Comput Chem* 25:1605–1612.
5. Edwards MJ, et al. (2015) Redox linked flavin sites in extracellular decaheme proteins involved in microbe-mineral electron transfer. *Sci Rep* 5:11677.
6. Firer-Sherwood MA, Ando N, Drennan CL, Elliott SJ (2011) Solution-based structural analysis of the decaheme cytochrome, MtrA, by small-angle X-ray scattering and analytical ultracentrifugation. *J Phys Chem B* 115:11208–11214.
7. Gray HB, Winkler JR (2003) Electron tunneling through proteins. *Q Rev Biophys* 36: 341–372.
8. Blauch D, Saveant J (1992) Dynamics of electron hopping in assemblies of redox centers. Percolation and diffusion. *J Am Chem Soc* 114:3323–3332.
9. Ramadurai S, et al. (2009) Lateral diffusion of membrane proteins. *J Am Chem Soc* 131:12650–12656.
10. White GF, et al. (2013) Rapid electron exchange between surface-exposed bacterial cytochromes and Fe(III) minerals. *Proc Natl Acad Sci USA* 110:6346–6351.
11. Breuer M, Rosso KM, Blumberger J (2014) Electron flow in multiheme bacterial cytochromes is a balancing act between heme electronic interaction and redox potentials. *Proc Natl Acad Sci USA* 111:611–616.

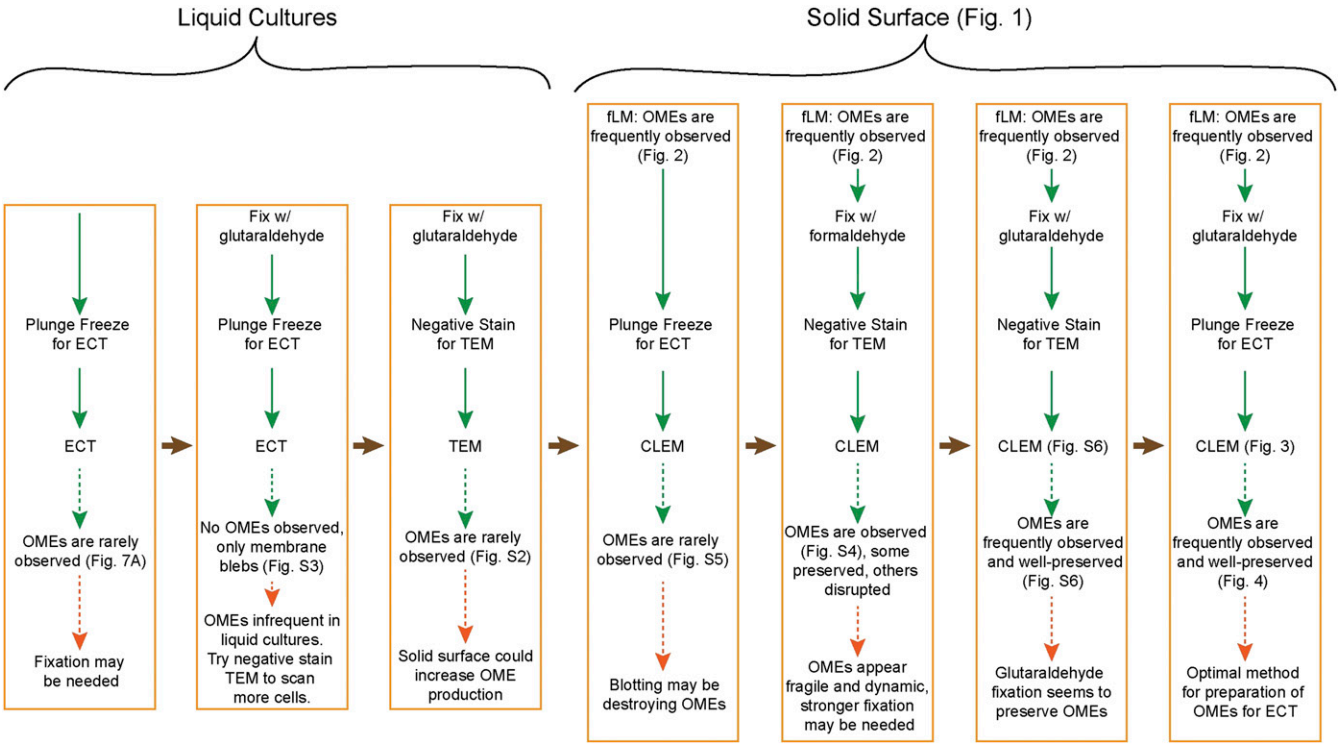

Fig. S1. Summary of the sample preparation methods attempted in this work for transmission electron microscopy studies of *S. oneidensis* OM extensions. Different experimental methods are listed in the sequence in which they were attempted (*Left* to *Right*) based on the result from the previous column. "Liquid Cultures" (*Left*) refers to growing cells in liquid cultures using a batch culture or a chemostat, whereas "Solid Surface" (*Right*) indicates OM extensions produced by cells on an EM grid in the perfusion flow imaging platform. Within each column, a specific set of experimental methodologies, the resulting observation, and our interpretation of the results are marked by solid green, dashed green, and dashed orange arrows, respectively.

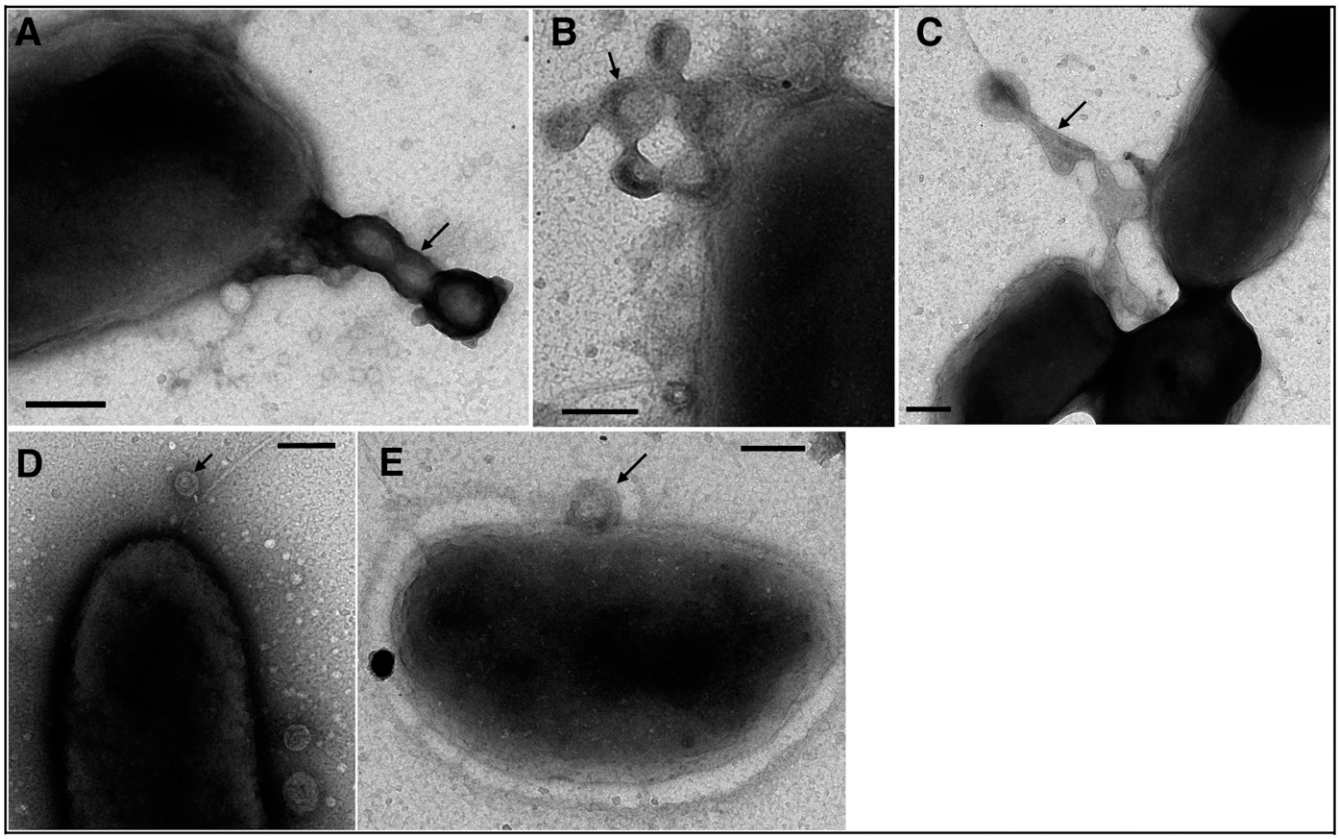

Fig. S2. TEM images of negative stained, glutaraldehyde-fixed *S. oneidensis* cells from the chemostat method of growth (corresponds to column 3 in Fig. S1, *Left*). (*A*–*C*) Images show the three OM extensions detected from the thousands of cells screened, indicating that OM extensions are rare in liquid cultures. (*D* and *E*) Single vesicles, which could be precursors to OM extensions, were seen budding from the cell or broken off from the cell. (Scale bars: 200 nm.)

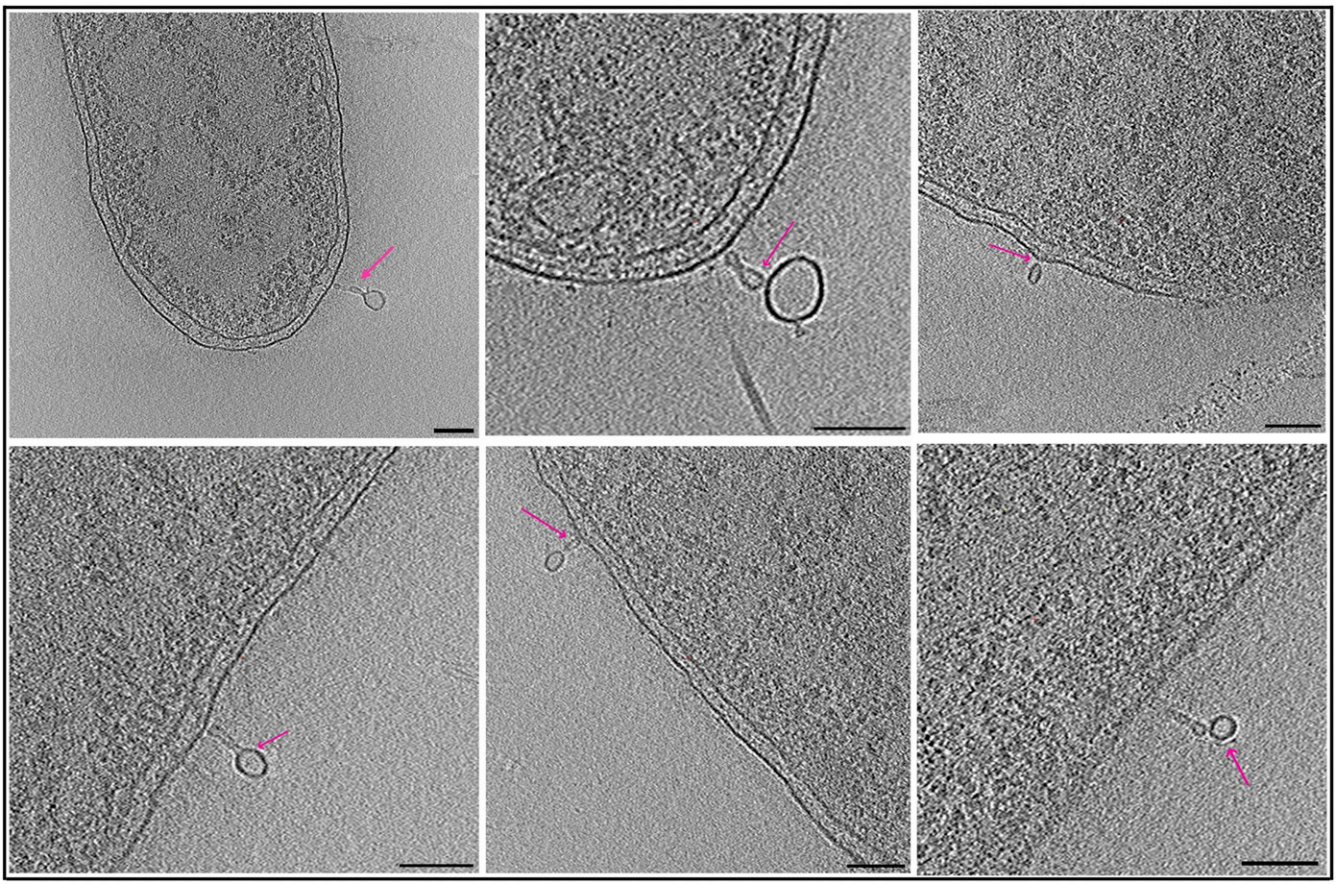

Fig. S3. ECT images of glutaraldehyde-fixed *S. oneidensis* cells grown using the serum bottle method frequently showed membrane blebs (arrows) (corresponds to column 2 in Fig. S1, *Left*). These membrane blebs, however, did not assemble into the typically long OMV chain morphology, and it was not clear whether they were artifacts of fixation or other sample preparation steps. (Scale bars: 100 nm.)

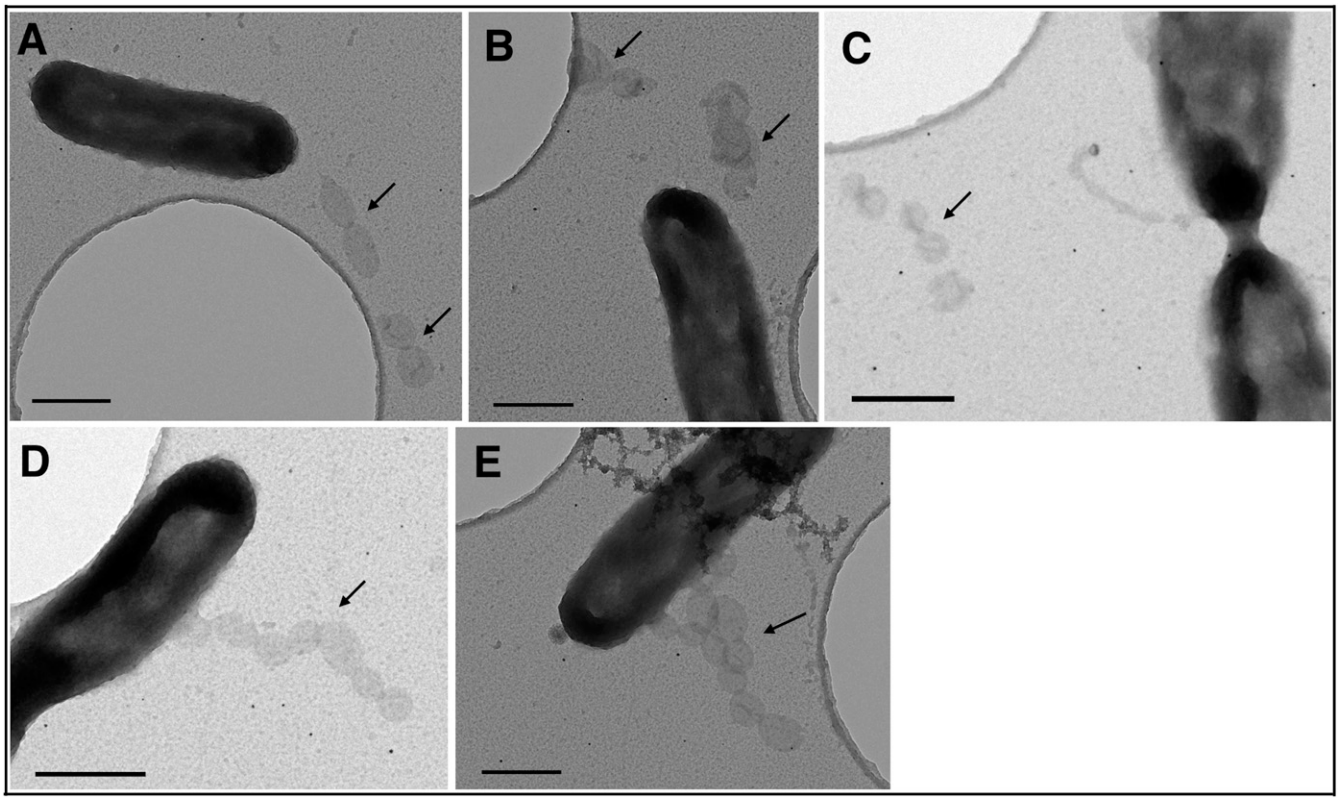

Fig. S4. TEM images of negative stained, formaldehyde-fixed *S. oneidensis* cells from the perfusion flow imaging platform (corresponds to column 2 in Fig. S1, *Right*). (*A*–*C*) Presumed disrupted OM extensions (arrows) that were not sufficiently preserved with formaldehyde fixation. (*D* and *E*) While formaldehyde fixation did not preserve all OM extensions, some of them were preserved (arrows). (Scale bars in *A*–*E*: 0.5 μm.)

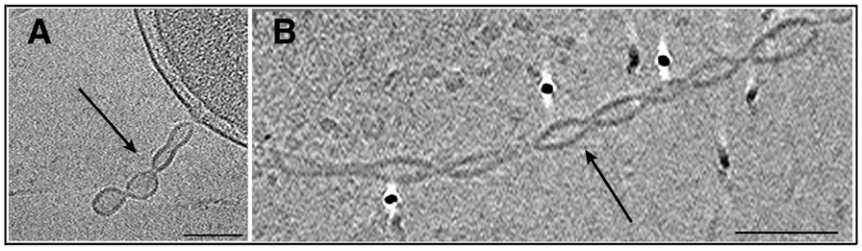

Fig. S5. (*A* and *B*) Two unfixed OM extensions (arrows) from the perfusion flow imaging platform that remained intact until ECT imaging. These images are from a *S. oneidensis* Δ*crp* mutant (lacking the cAMP receptor protein). The OMV chain morphology seen here confirms that this morphology is not an artifact of fixation (corresponds to column 1 in Fig. S1, *Right*). (Scale bars: 100 nm.)

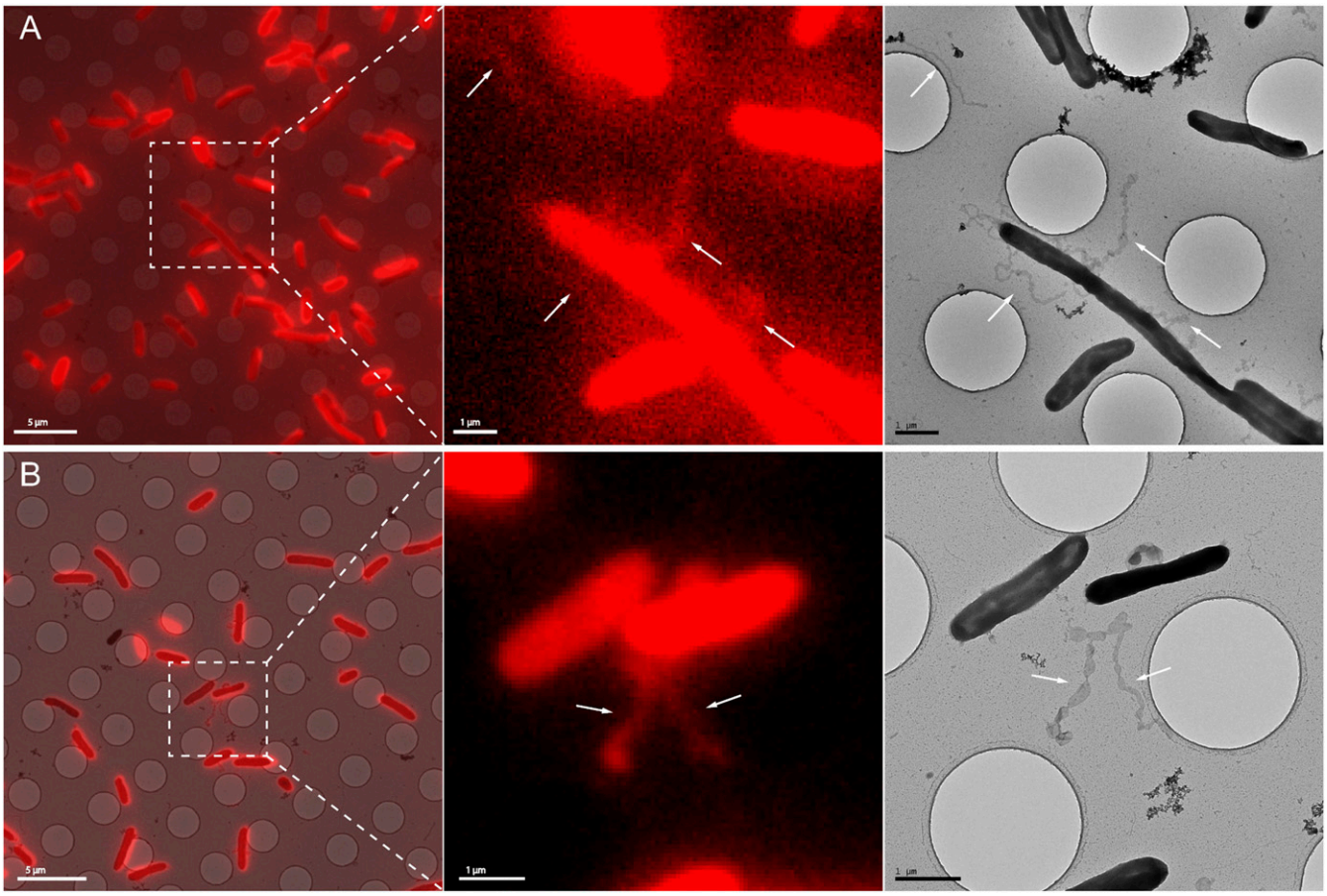

Fig. S6. Correlative fLM and negative stained, glutaraldehyde-fixed TEM images of *S. oneidensis* OM extensions from the perfusion flow imaging platform (corresponds to column 3 in Fig. S1, *Right*). *A* and *B* are *S. oneidensis* wild type and *S. oneidensis* Δ*crp* and correspond to Movies S1 and S2, respectively. (*A* and *B*, *Left*) Overlay of the fLM and TEM images. (*A* and *B*, *Center* and *Right*) Enlarged fLM and TEM views of the areas in the white dashed boxes, respectively. White arrows indicate the OM extensions.

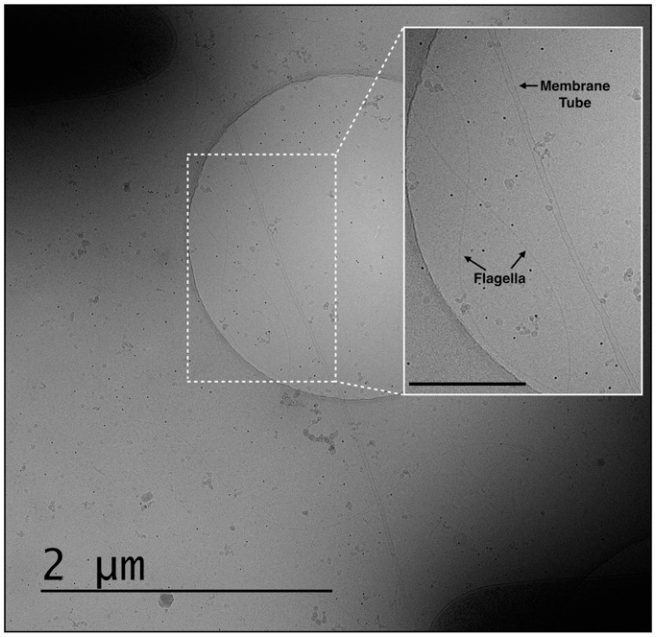

Fig. S7. Cryo-EM projection image of a smooth membrane filament of *S. oneidensis* from the perfusion flow imaging platform. Next to the filament are flagella that have been marked for comparison. *Inset* is an enlarged view of the boxed region. (*Inset* scale bar: 500 nm.)

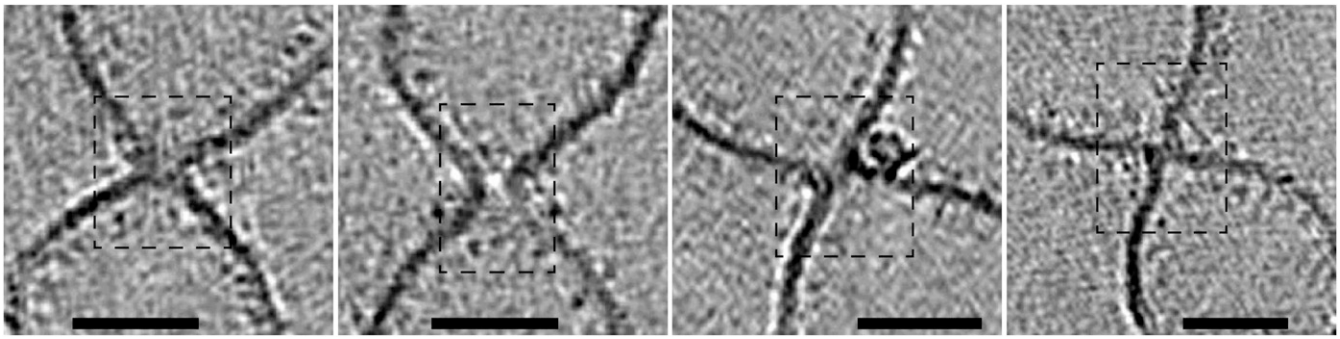

Fig. S8. Enlarged views of constriction points from the unfixed near-native OM extension in Fig. 4*C*. Dashed black boxes highlight the presence of densities at four different junctions that connect vesicles along the OMV chain. (Scale bars: 50 nm.)

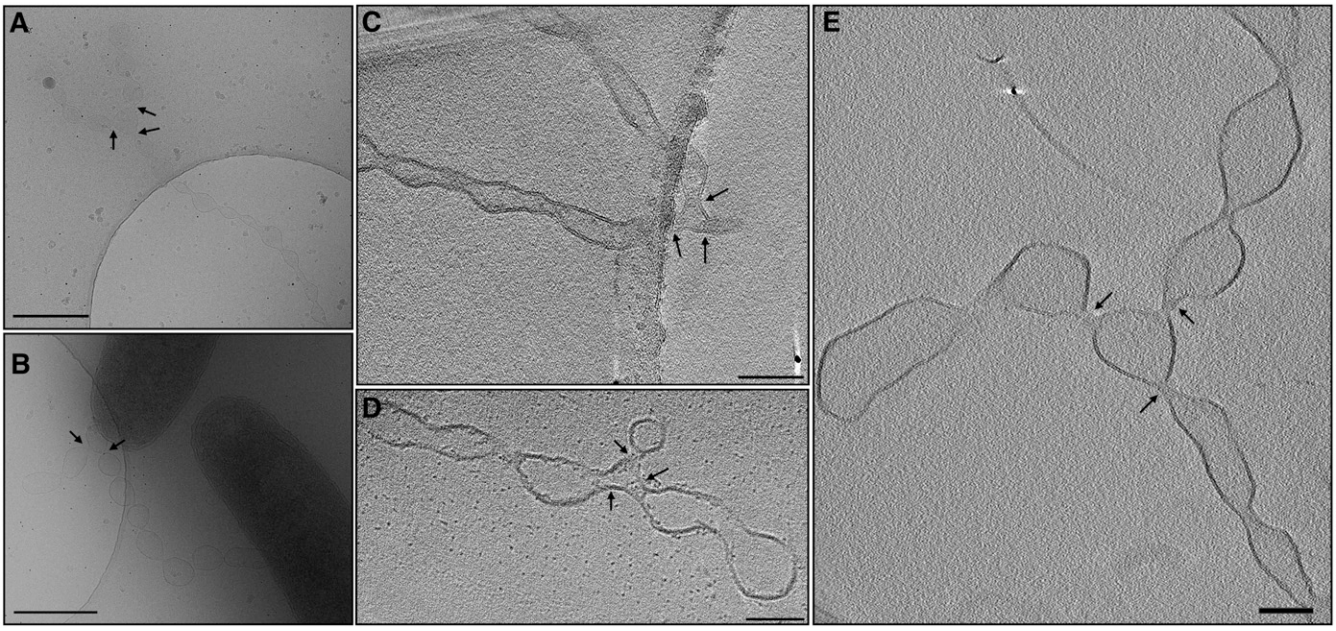

Fig. S9. (*A*–*E*) Branching of OMV chains from the perfusion flow imaging platform shown in (*A* and *B*) cryo-EM projection images and (*C*–*E*) ECT images. (Scale bars in *A* and *B*, 500 nm; in *C*–*E*, 100 nm.) Arrows indicate the branching points. *A*–*D* are *S. oneidensis* wild type and *E* is *S. oneidensis* Δ*crp* mutant. Movie S13 corresponds to *D*.

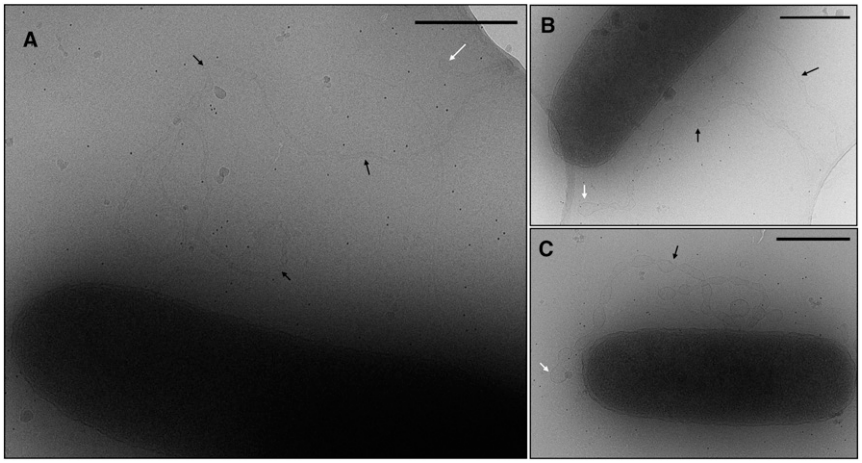

Fig. S10. (*A*–*C*) Three examples of Cryo-EM projection images of *S. oneidensis* OM extensions from the perfusion flow imaging platform showing they are flexible, increasing the likelihood of contacting terminal EAs. Black arrows point to the OM extensions and white arrows indicate the end of the OM extensions. (Scale bars: 500 nm.)

Table S1. Strains used in this study

Strain	Relevant genotype	Ref.
S. oneidensis MR-1	Wild type	(1)
S. oneidensis, ΔMtr/Δ*mtrB*/Δ*mtrE*	Δ*mtrB*/Δ*mtrE*/Δ*mtrC*/Δ*omcA*/Δ*mtrF*/Δ*mtrA*/Δ*mtrD*/Δ*dmsE*/Δ*SO4360*/Δ*cctA*/Δ*recA*	(2)
S. oneidensis Δ*flg*	Lacking flagellin genes SO_3237 and SO_3238	(3)
S. oneidensis Δ*crp*	Lacking the cAMP receptor protein (CRP)	(4)

1. Myers CR, Nealson KH (1988) Bacterial manganese reduction and growth with manganese oxide as the sole electron acceptor. *Science* 240:1319–1321.
2. Coursolle D, Gralnick JA (2012) Reconstruction of extracellular respiratory pathways for iron(III) reduction in *Shewanella oneidensis* strain MR-1. *Front Microbiol* 3:56.
3. Bouhenni R, et al. (2010) The role of *Shewanella oneidensis* MR-1 outer surface structures in extracellular electron transfer. *Electroanalysis* 22:856–864.
4. Charania MA, et al. (2009) Involvement of a membrane-bound class III adenylate cyclase in regulation of anaerobic respiration in *Shewanella oneidensis* MR-1. *J Bacteriol* 191:4298–4306.

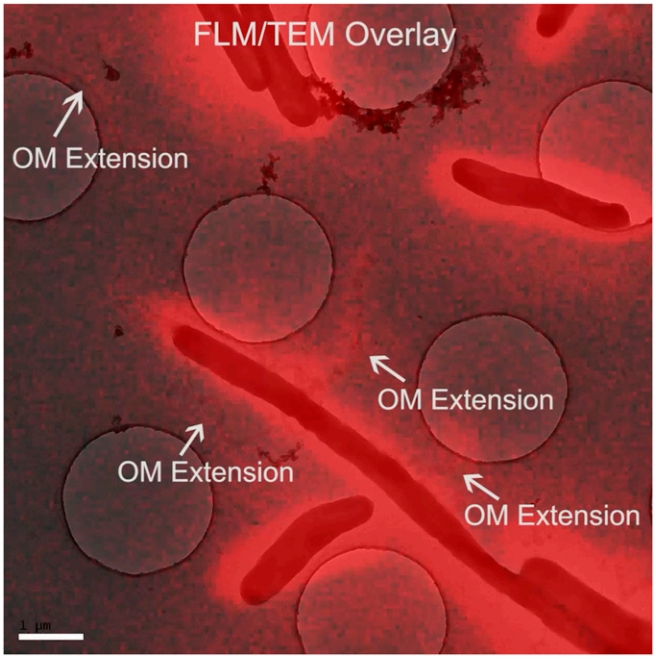

Movie S1. Correlative fLM and negative stained, glutaraldehyde-fixed TEM of *S. oneidensis* OM extensions from the perfusion flow imaging platform (corresponds to Fig. S6*A*). fLM and TEM images of a field of view with cells are shown first, followed by an overlay of the two images highlighting their correlation. A specific cell with OM extensions is then enlarged and subsequent correlative TEM reveals the OMV chain architecture of OM extensions not visible in fLM. Red fluorescence is the result of membrane staining by FM 4-64FX.

Movie S1

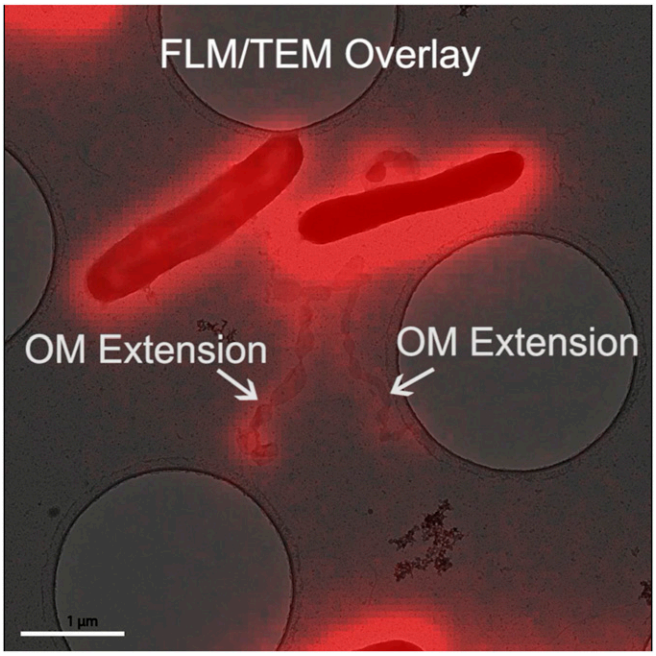

Movie S2. Correlative fLM and negative stained, glutaraldehyde-fixed TEM of *S. oneidensis* Δ*crp* OM extensions (corresponds to Fig. S6*B*). fLM and TEM images of a field of view with cells are shown first, followed by an overlay of the two images highlighting their correlation. A specific cell with an OM extension is then enlarged and subsequent correlative TEM reveals the OMV chain architecture of OM extensions not visible in fLM. Red fluorescence is the result of membrane staining by FM 4-64FX.

Movie S2

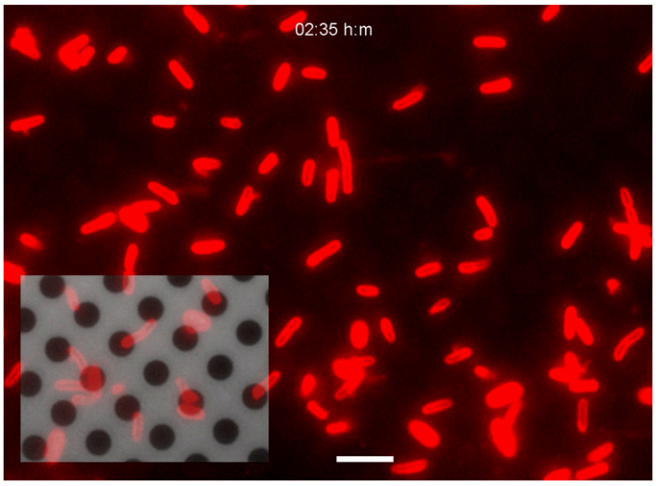

Movie S3. Time-lapse movie of *S. oneidensis* OM extension growth on an EM grid in the perfusion flow imaging platform (corresponds to Fig. 2). *Inset* is an overlap of red fluorescence and reflective brightfield channels, revealing both the holey carbon film coating the EM grid and the fluorescently labeled cells attached to it. (Scale bar: 5 µm.) Red fluorescence is the result of membrane staining by FM 4-64FX. The interval between two consecutive frames is 5 min, but is reduced to 333 ms (three frames per second). Real time is shown at the top in hours and minutes (h:m).

Movie S3

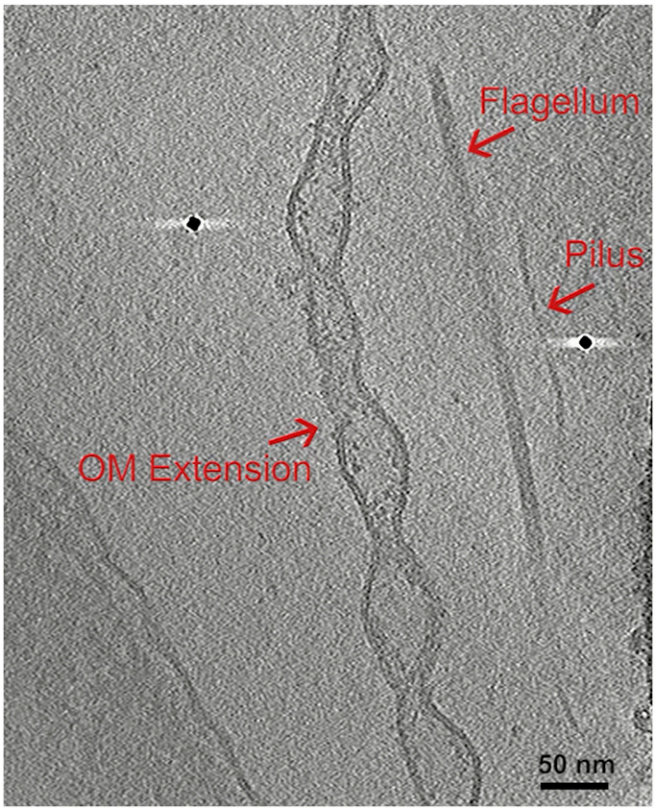

Movie S4. The 3D reconstruction of an OM extension, a flagellum, and a pilus from *S. oneidensis*, allowing direct comparison of their sizes and morphologies (corresponds to Fig. 4*D*). The 3D reconstruction (tomogram) is shown slice by slice.

Movie S4

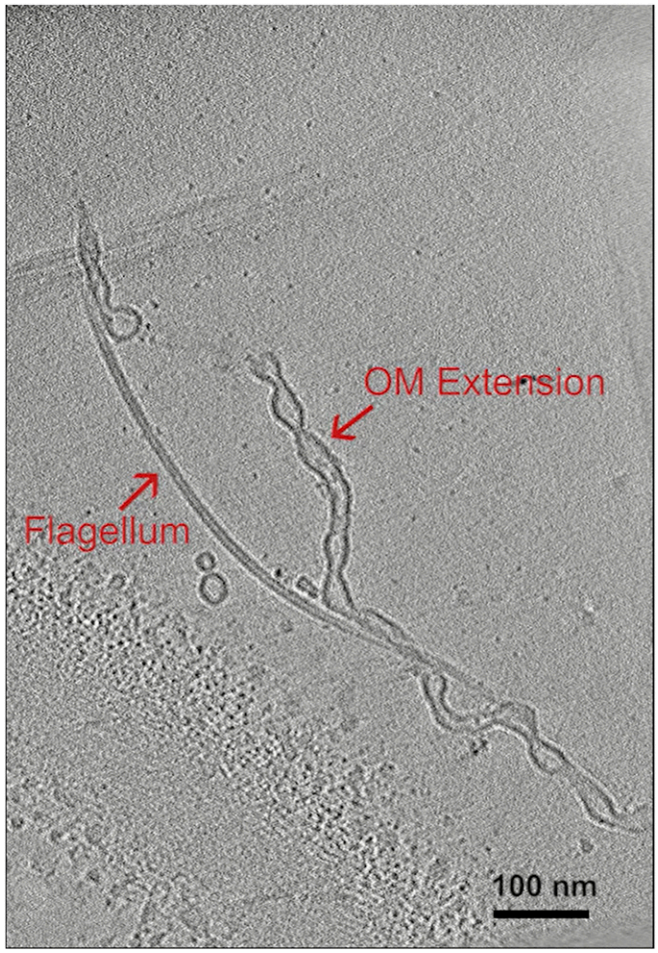

Movie S5. The 3D reconstruction of a thin OM extension and a flagellum from *S. oneidensis* (corresponds to Fig. 4*F*) allowing direct comparison of their dimensions. The 3D reconstruction (tomogram) is shown slice by slice.

Movie S5

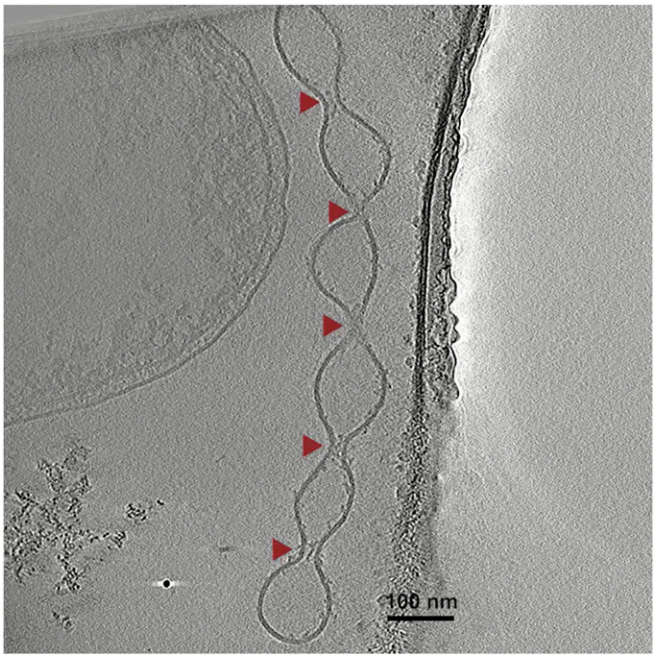

Movie S6. The 3D reconstruction of a *S. oneidensis* OM extension, highlighting the "junction densities" (corresponds to Fig. 5*A*). Arrowheads point to constriction points along the OMV chain. The junction densities at three enlarged constriction points are circled in red. These densities are proposed to facilitate the constriction of the membrane on the OM extension interior. The 3D reconstruction (tomogram) is shown slice by slice.

Movie S6

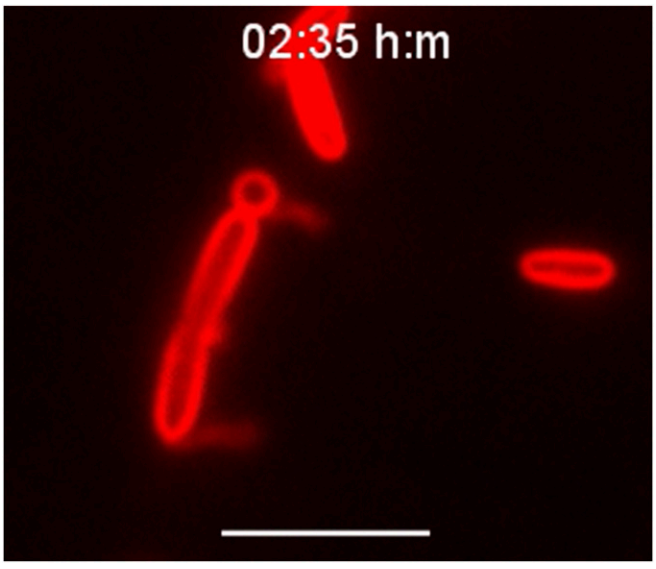

Movie S7. Time-lapse movie of OM extension growth and retraction by *S. oneidensis* Δ*flg*. OMV chains grow from a cell and are later retracted to form single large vesicles at the growth initiation points (corresponds to Fig. 5*B*). (Scale bar: 5 μm.) Red fluorescence is the result of membrane staining by FM 4-64FX. The interval between two consecutive frames is 5 min, but is reduced to 333 ms (three frames per second). Real time is shown at the top in hours and minutes (h:m).

Movie S7

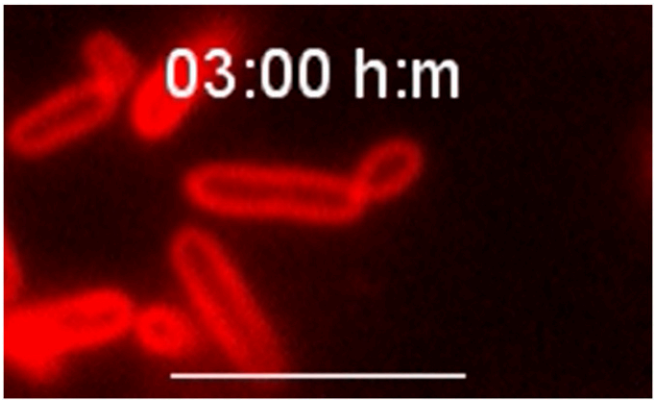

Movie S8. Time-lapse movie of OM extension growth and retraction by *S. oneidensis* wild-type. An OMV chain grows from a cell and is later retracted to form a single large vesicle at the growth initiation point. (Scale bar: 5 μm.) Red fluorescence is the result of membrane staining by FM 4–64FX. The interval between two consecutive frames is 5 min, but is reduced to 333 ms (3 frames per second). Real time is shown at the top in hours and minutes (h:m).

Movie S8

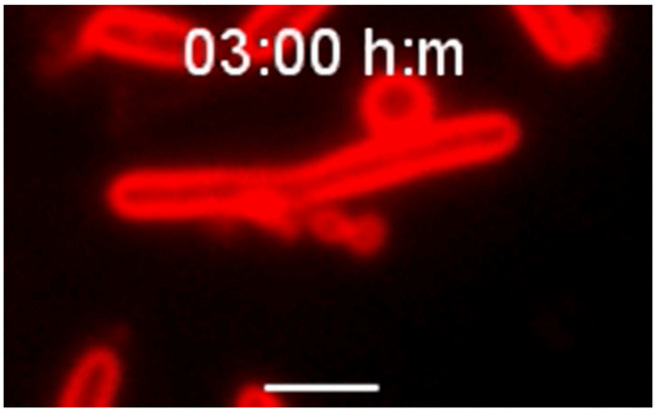

Movie S9. Time-lapse movie of *S. oneidensis* wild-type OM extension growth and transformation. An OM extension grows from a cell as an OMV chain composed of large vesicles and is later transformed into a smoother form (corresponds to Fig. 5C). (Scale bar: 2 μm.) Red fluorescence is the result of membrane staining by FM 4-64FX. The interval between two consecutive frames is 5 min, but is reduced to 333 ms (three frames per second). Real time is shown at the top in hours and minutes (h:m).

Movie S9

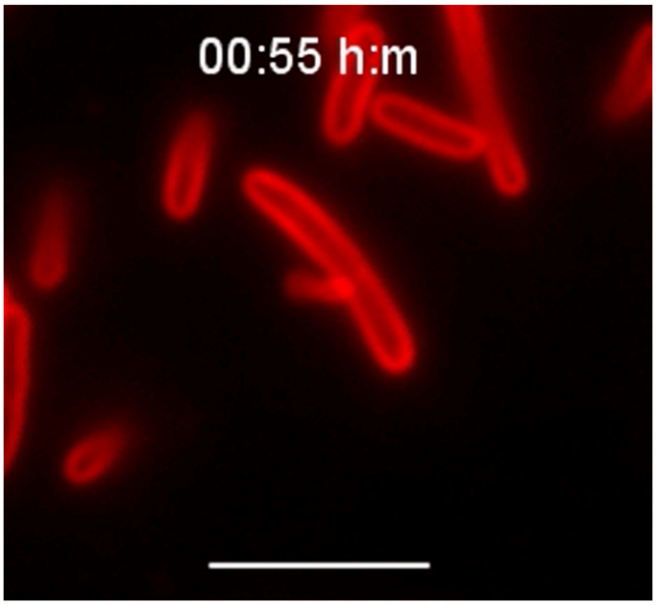

Movie S10. Time-lapse movie of *S. oneidensis* wild-type OM extension growth and transformation. An OM extension alternates between smooth OMV chain and large vesicle-chain forms. (Scale bar: 5 μm.) Red fluorescence is the result of membrane staining by FM 4-64FX. The interval between two consecutive frames is 5 min, but is reduced to 333 ms (three frames per second). Real time is shown at the top in hours and minutes (h:m).

Movie S10

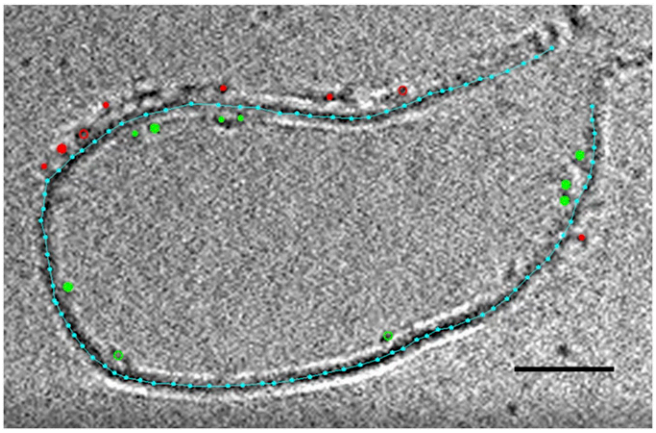

Movie S11. The 3D reconstruction of the vesicle shown in Fig. 6*C*. Membrane (cyan line), interior particles (green circles), and exterior particles (red circles) are labeled as model points. Meshed view of the membrane is generated and all of the observed interior and exterior densities are shown as model points in 3D. The 3D reconstruction (tomogram) is shown slice by slice. (Scale bar: 50 nm.)

Movie S11

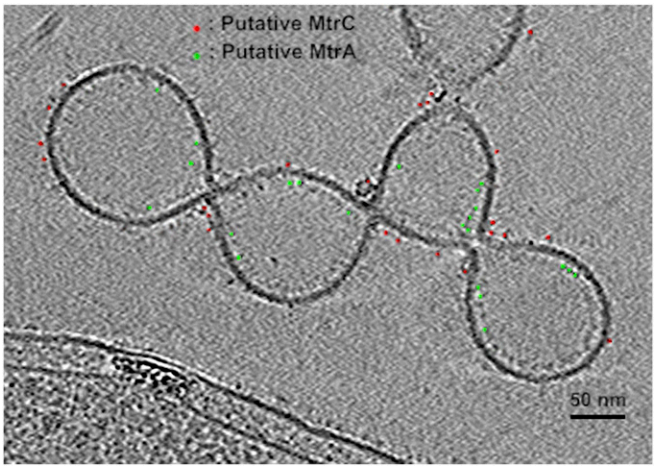

Movie S12. The 3D reconstruction of an unfixed OM extension from *S. oneidensis* wild type with all of the observed interior (putative MtrA) and exterior (putative MtrC) densities marked as model points in green and red, respectively (corresponds to Fig. 7*A*). Also shown is the 3D isosurface view of the OM extension with the putative EET proteins (corresponds to Fig. 7*C*). The 3D reconstruction (tomogram) is shown slice by slice.

Movie S12

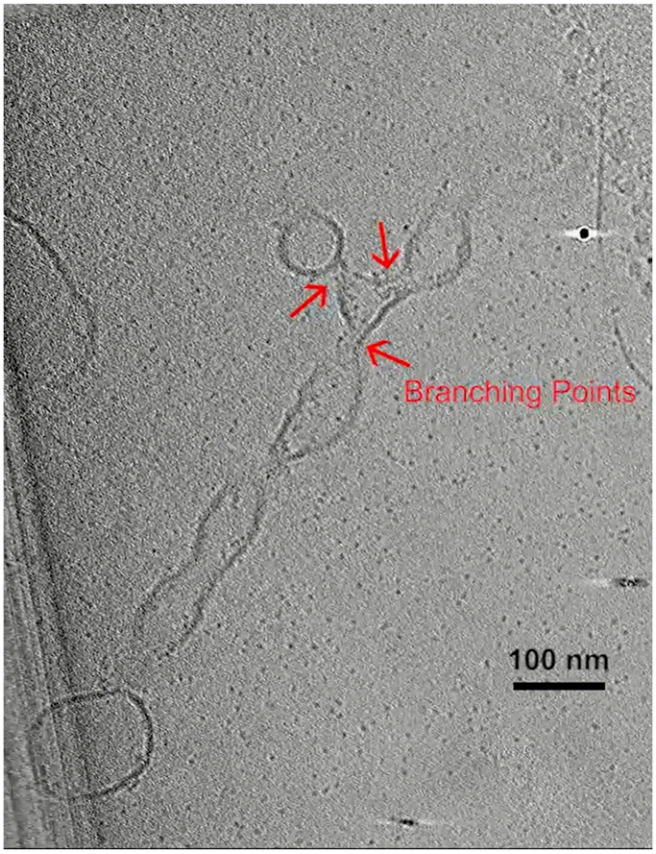

Movie S13. OMV chain branching demonstrated by ECT of *S. oneidensis* (corresponds to Fig. S9*D*). The 3D reconstruction (tomogram) is shown slice by slice.

Movie S13